Numerical study of initial perturbation effects on Richtmyer-Meshkov instability in nonuniform flows

Jia-xin Xiao, Jing-song Bai,* and Tao Wang
Institute of Fluids Physics, China Academy of Engineering Physics, Mianyang 621900 Sichuan, People's Republic of China
(Received 23 April 2016; revised manuscript received 23 June 2016; published 22 July 2016)

The effects of an initial perturbation on Richtmyer-Meshkov instability are numerically studied by simulating the process of incident shock (Ma = 1.27) impacting different groups of initial multimode cosine interfaces formed by different amplitudes in initially nonuniform flows whose density is a Gaussian function. The numerical results indicate that the evolution of the interface with a large initial amplitude in a low-density nonuniform area grows fastest, while that with a small initial amplitude in a high-density nonuniform area grows slowly. Further analysis of vorticity and circulation illustrates these phenomena. The interface with a large initial amplitude in a low-density zone possesses a larger density gradient, which results in a larger amount of vorticity and circulation, leading to the fast-changing evolution of the interface. Distinctive evolution mechanisms of Richtmyer-Meshkov instability between the nonuniform flows and the uniform flows are analyzed in detail.

DOI: 10.1103/PhysRevE.94.013112

I. INTRODUCTION

The Richtmyer-Meshkov instability occurs when a shock traverses a perturbed interface between two fluid layers, depositing vorticity on the interface. The key mechanism of this instability is the baroclinic vorticity production due to the misalignment between the pressure and the density gradients $(\vec{\nabla}\rho \times \vec{\nabla} p)/\rho^2 \neq 0$. This instability is of great significance both for fundamental research and for engineering application in a number of research fields, including the fuel mixing in scramjet combustion [1], astrophysical flows such as supernova [2], and molecular clouds in the interstellar medium, the inertial confinement fusion [3].

Recent decades have seen numerous investigations of interface instability in theoretical research, numerical simulation, and experimental study, all of which indicate that initial conditions have important effects on the evolution of interface instability. Yang *et al.* [1] numerically simulated the vertical flows to improve the efficient mixing of fuel and oxidizer in a scramjet and finally confirmed seven initial factors that greatly affect the mixing. Kumar *et al.* [4] argued that small variation of initial conditions could lead to distinct morphologies. Orlicz *et al.* [5] conducted the heavy-gas curtain experiments using different Mach numbers, which indicated that increased Mach number results in faster evolution of interface instability.

According to most previous studies, the initial flows are assumed to be uniform, while the actual flows in some experiments and practical applications tend to be nonuniform. In addition to that, research of interface instability in variable density flows is a priority research direction in the Matter-Radiation Interactions in Extremes plan [6] of the Los Alamos National Laboratory. Liu *et al.* [7] experimentally studied Richtmyer-Meshkov instability in SF_6 nonuniform flows and presented a view that the evolution of flow disturbance grows faster in a low-density zone due to the initial density nonuniformity. Bai *et al.* [8] determined that the initial density distribution of the experiment of Liu *et al.* was a Gaussian function through numerical simulation and then reproduced the experimental process. The follow-up study of Bai *et al.* [9] showed that the nonuniformity of initial flows has greater effects on the linear regime of Richtmyer-Meshkov instability evolution than on that in the nonlinear regime.

Based on our previous work and in light of others' works, the present work investigates the effects of initial perturbations on Richtmyer-Meshkov instability via numerical simulations. Simulations of incident shock (Ma = 1.27) impacting multimode cosine interfaces formed by different amplitudes are performed under the conditions of uniform flows and nonuniform flows. Afterward, a quantitative analysis of amplitude, vorticity, and circulation is presented to demonstrate the effects of nonuniformity, initial amplitude, and density on the evolution of interface instability. The results of our simulation and detailed analysis are expected to explain the previous experiment [7] and figure out the mechanism of interface instability in nonuniform flows. Meanwhile, it is significant to offer meaningful and prospective guidelines to the related numerical, theoretical modeling, and experiments of such complex flows.

II. NUMERICAL METHODS

The simulations are run with a large-eddy simulation code MVFT (multiviscous flow and turbulence), which can be utilized to simulate accurately the process of shock impinging the material interface in multiviscous fluid. Based on the multiviscous fluid piecewise parabolic method, MVFT applies the Vreman subgird eddy viscosity model [10] to the solution of the Navier-Stokes equations:

$$\begin{aligned}
&\frac{\partial \bar{\rho}}{\partial t} + \frac{\partial \bar{\rho}\tilde{u}_j}{\partial x_j} = 0,\\
&\frac{\partial \bar{\rho}\tilde{u}_i}{\partial t} + \frac{\partial \bar{\rho}\tilde{u}_j\tilde{u}_i}{\partial x_j} + \frac{\partial \bar{p}}{\partial x_i} = \frac{\partial(\bar{\sigma}_{ij} + \tau_{ij})}{\partial x_j},\\
&\frac{\partial \bar{\rho}\tilde{E}}{\partial t} + \frac{\partial(\bar{\rho}\tilde{u}_j\tilde{E} + \bar{p}\tilde{u}_j)}{\partial x_j} = -\frac{\partial(\bar{q}_j + Q_j)}{\partial x_j} + \frac{\partial[\tilde{u}_i(\bar{\sigma}_{ij} + \tau_{ij})]}{\partial x_j},\\
&\frac{\partial \bar{Y}^{(s)}}{\partial t} + \tilde{u}_j\frac{\partial \bar{Y}^{(s)}}{\partial x_j} = \frac{\partial}{\partial x_j}\left(\tilde{D}\frac{\partial \bar{Y}^{(s)}}{\partial x_j}\right),\\
&\qquad s = 1,2,3,\ldots,N-1, \qquad (1)
\end{aligned}$$

*bjsong@foxmail.com

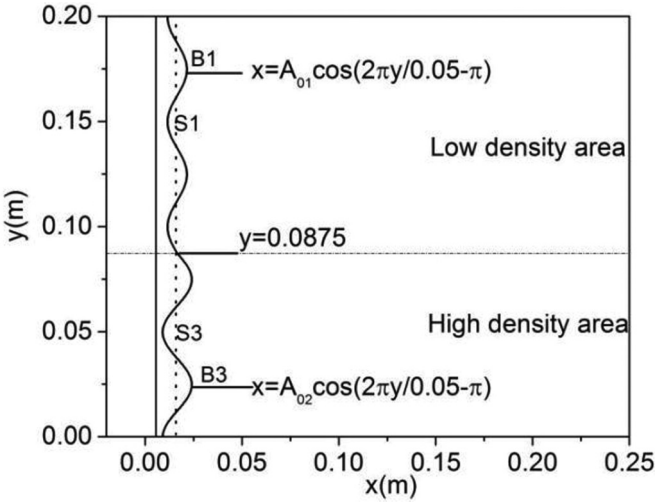

FIG. 1. Initial structure diagram.

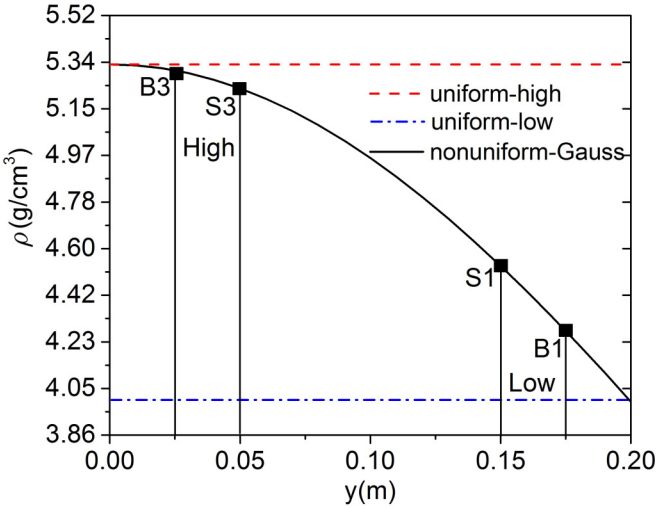

FIG. 2. Density profiles of nonuniform flows with a Gaussian function and uniform flows in the vertical direction.

where i and j are the three directions of x and y. When i is equal to j, the tensor add operations are used. Here $\bar{\rho}$, $\tilde{u}_k$, and $\bar{p}$ stand for the resolved-scale fluid density, the velocity, and the pressure; $\bar{E}$ represents the total energy per unit mass; N refers to the types of fluids; $\bar{Y}^{(s)}$ is the volume fraction of the sth fluids; $\tilde{D}$ is the diffusion coefficient, which can be calculated by $D = \upsilon/S_c$, with υ the fluid viscosity and S_c the Schmidt number; $\bar{\sigma}_{ij} = \mu_l[\partial\,\tilde{u}_i/\partial\,x_j + \partial\,\tilde{u}_j/\partial\,x_i - 2/3\delta_{ij}(\partial\,\tilde{u}_k/\partial\,x_k)]$ is the Newtonian fluid viscous stress tensor; $\tau_{ij} = \rho(\tilde{u}_i\tilde{u}_j - \widetilde{u_i u_j})$ is the subgrid scale stress tensor; and $\bar{q}_j = -\lambda_l\partial T/\partial x_j$ ($\lambda_l = \mu_l c_p/\mathrm{Pr}_l$) and $Q_j = -\lambda_t\partial T/\partial x_j$ ($\lambda_t = \mu_t c_p/\mathrm{Pr}_t$) are the energy flux per unit time and space in resolved and subgrid scales, respectively, with μ_l the fluid viscosity, c_p the specific heat of fluid, and Pr the Prandtl number. The equation of state adopts the ideal gas state form.

The operator splitting technique is used to decompose the physical process into three subprocesses: the calculation of inviscid flux, viscous flux, and heat flux. Then the two-step Lagrange-remap algorithm is applied to calculate the inviscid flux in one step time, divided into the following four steps: (1) the piecewise parabolic interpolation of physical quantities, (2) the approximate solution of the Riemann problems, (3) the solution of the evolution of Lagrange equations, and (4) the remapping of the physical quantities to the stationary Euler meshes. As for the viscous flux and the heat flux, the second-order spatial center difference and two-step Runge-Kutta time marching method are applicable. More details can be obtained from previous studies [11].

TABLE I. Seven groups of initial amplitudes.

No.	A_{01}	A_{02}
1	5	7.5
2	7.5	5
3	2.5	7.5
4	7.5	2.5
5	7.5	7.5
6	7.5	10
7	10	7.5

III. RESULTS AND DISCUSSION

A. Initial conditions

Based on our previous work [7], the flow field consists of air and SF_6 separated by a multimode cosine interface whose wavelength is 0.05 m and whose equilibrium position of perturbation is $x = 0.016$ m. The initial structure diagram is shown in Fig. 1, where B1 and S1 are the peak and the trough of the initial amplitude A_{01} perturbation and B3 and S3 are the peak and the trough of the initial amplitude A_{02} perturbation. The interface perturbation function can be described by the following equations:

$$x = \begin{cases} A_{01}\cos(2\pi y/0.05 - \pi), & 0.0875 < y < 0.2 \\ A_{02}\cos(2\pi y/0.05 - \pi), & 0 < y < 0.0875. \end{cases} \quad (2)$$

The seven groups of different amplitudes are presented in Table I.

A shock wave with the strength $\mathrm{Ma} = 1.27$ is initialized in the light gas air, whose front is located at $x = 5.56 \times 10^{-3}$ m. For the initial nonuniform SF_6 flow field, the Gaussian function is used to present the initial SF_6 gas density, so we have

$$\rho(y) = \rho_{SF_6} e^{-[(y-y_c)^2/\delta^2]}, \quad \delta = 0.3729m, \quad y_c = 0. \quad (3)$$

Equation (3) would be made more distinct by plotting the profile of the density in Fig. 2, where the density of the bubble and spike is pinpointed.

The computational domain is $[-0.02\ \mathrm{m}, 0.25\ \mathrm{m}] \times [0.0\ \mathrm{m}, 0.2\ \mathrm{m}]$, discretized into 540×400 grids with the infinite condition to the right boundary and the solid wall to

TABLE II. Initial properties of air and SF_6.

Gas	Density (kg/m^3)	Specific heat ratio	Kinematic viscosity (10^{-6} m^2/s)	Prandtl number	Diffusion coefficient in air (cm^2/s)
air	1.29	1.40	15.5	0.71	0.204
SF_6	5.34	1.09	18.2	0.90	0.097

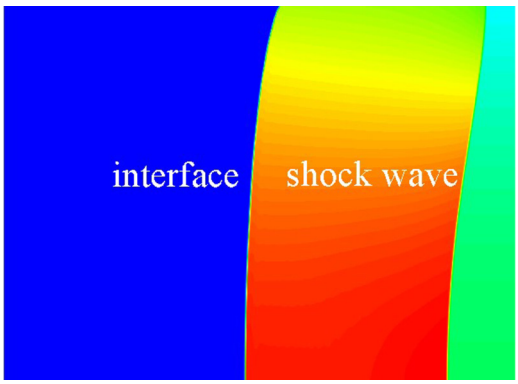

FIG. 3. Density contour images of the numerical simulation result in a nonuniform Gaussian function flow without initial perturbation on the interface.

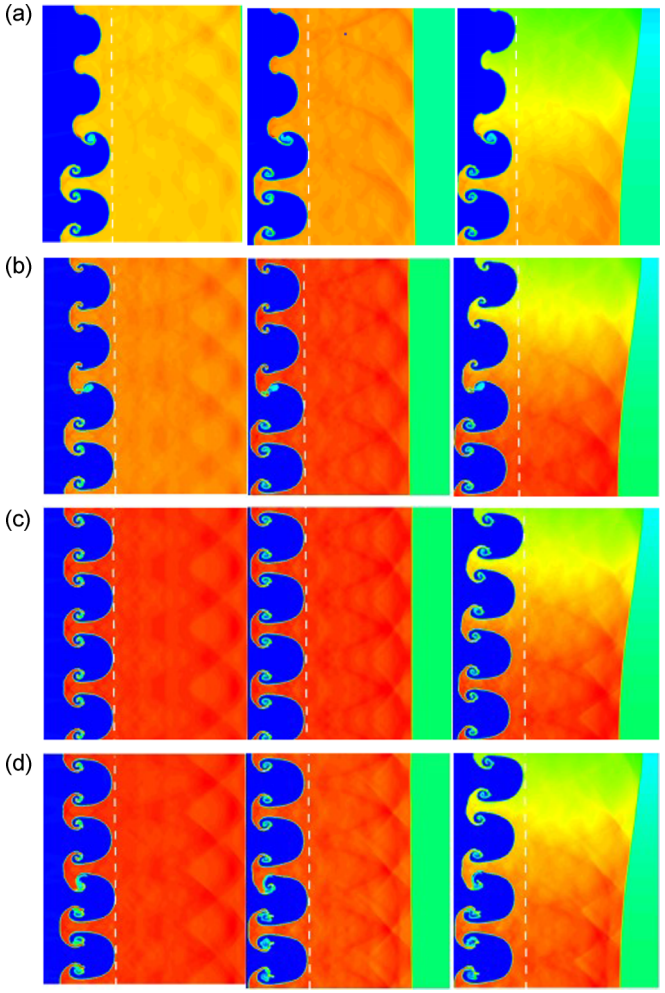

FIG. 4. Density contour images of the numerical simulation result at $t = 1$ ms under different groups of initial amplitudes: (a) ($A_{01} = 2.5$ mm-$A_{02} = 7.5$ mm), (b) ($A_{01} = 5.0$ mm-$A_{02} = 7.5$ mm), (c) ($A_{01} = 7.5$ mm-$A_{02} = 7.5$ mm), and (d) ($A_{01} = 7.5$ mm-$A_{02} = 10.0$ mm). The left column shows low-density uniform flows; the middle column, high-density uniform flows; and the right column, nonuniform Gaussian function flows.

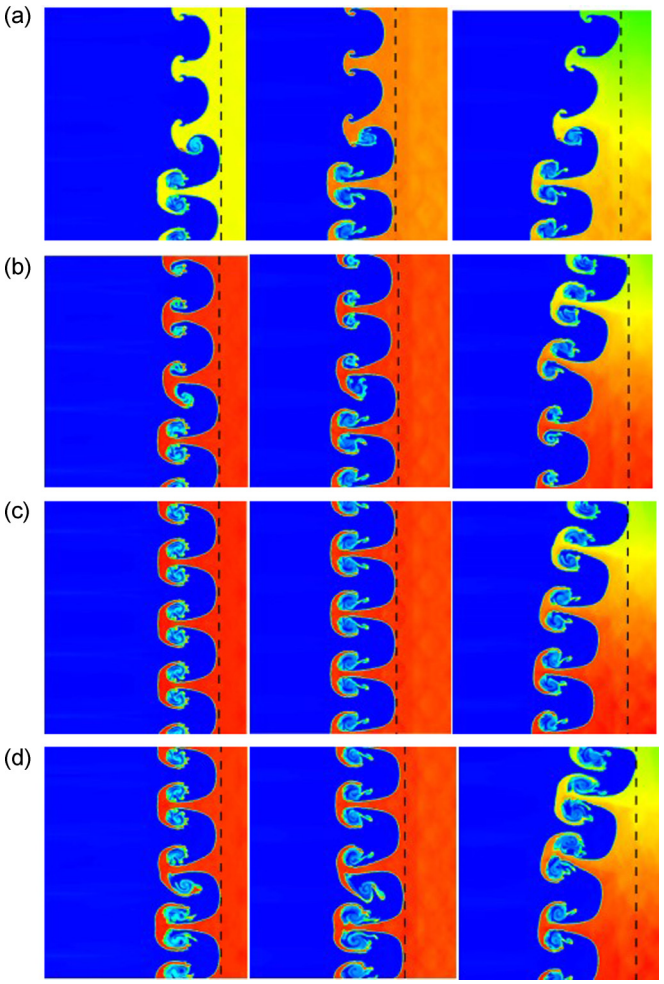

FIG. 5. Density contour images of the numerical simulation result at $t = 1.8$ ms under different groups of initial amplitudes: (a) ($A_{01} = 2.5$ mm-$A_{02} = 7.5$ mm), (b) ($A_{01} = 5.0$ mm-$A_{02} = 7.5$ mm), (c) ($A_{01} = 7.5$ mm-$A_{02} = 7.5$ mm), (d) ($A_{01} = 7.5$ mm-$A_{02} = 10.0$ mm). The left column shows the low-density uniform flows; the middle column, high-density uniform flows; and the right column, nonuniform Gaussian function flows.

the top and bottom boundaries. In order to obtain the nonlinear data, the total simulation time is fixed as 2 ms. Table II summarizes the properties of air and SF_6 gas at 1 atm pressure and 20 °C.

1. Flow visualizations

Visualizations of the density of the SF_6 gas contour of the numerical simulation results by MVFT are shown in Figs. 3–5 under different initial conditions. In order to study the influence of nonuniformity without initial perturbation on the interface, an additional simulation of shock impacting the straight interface in nonuniform flow can be visualized in Fig. 3. It is easy to notice the curvature in both the interface and shock wave at $t = 1$ ms due to the transverse gradient in the initial nonuniform flow field. This case is supposed to be comparable to and inspiring for the following studies.

As for Figs. 4 and 5, the left, middle, and right column images correspond with the low-density uniform flow

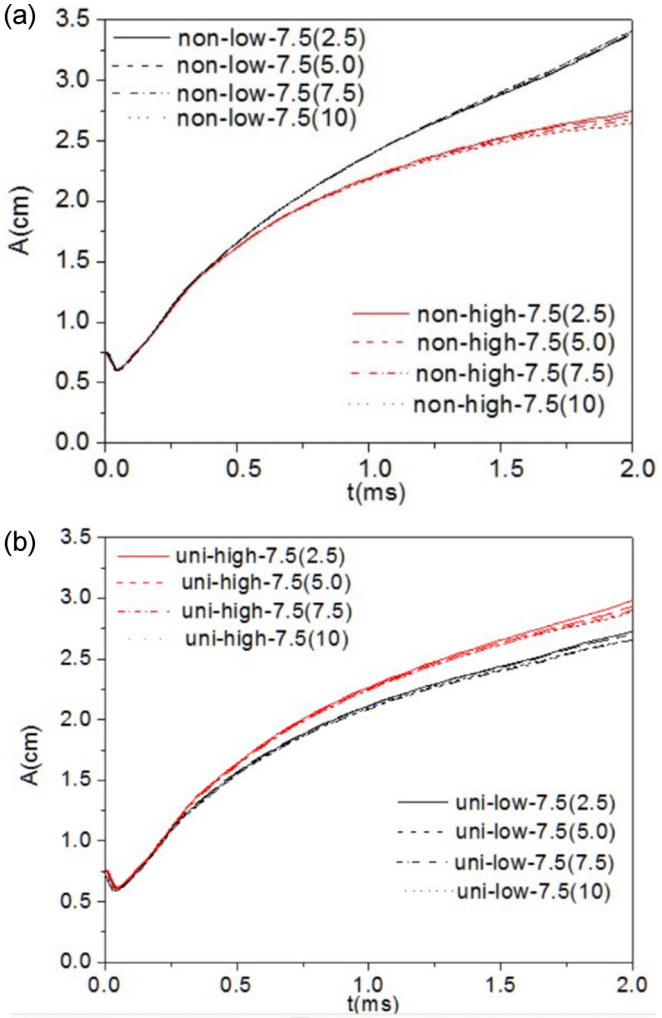

FIG. 6. Perturbation amplitude of $A_0 = 7.5$ mm initial amplitude with four other initial amplitudes: $A_0 = 2.5$ (solid line), 5.0 (dashed line), 7.5 (dash-dotted line), and 10.0 (dotted line) mm under four different flows: (a) low-density (black lines) zone and high-density [red (light gray) lines] zone in nonuniform flow and (b) low-density (black lines) zone and high-density [red (light gray) lines] zone in uniform flow.

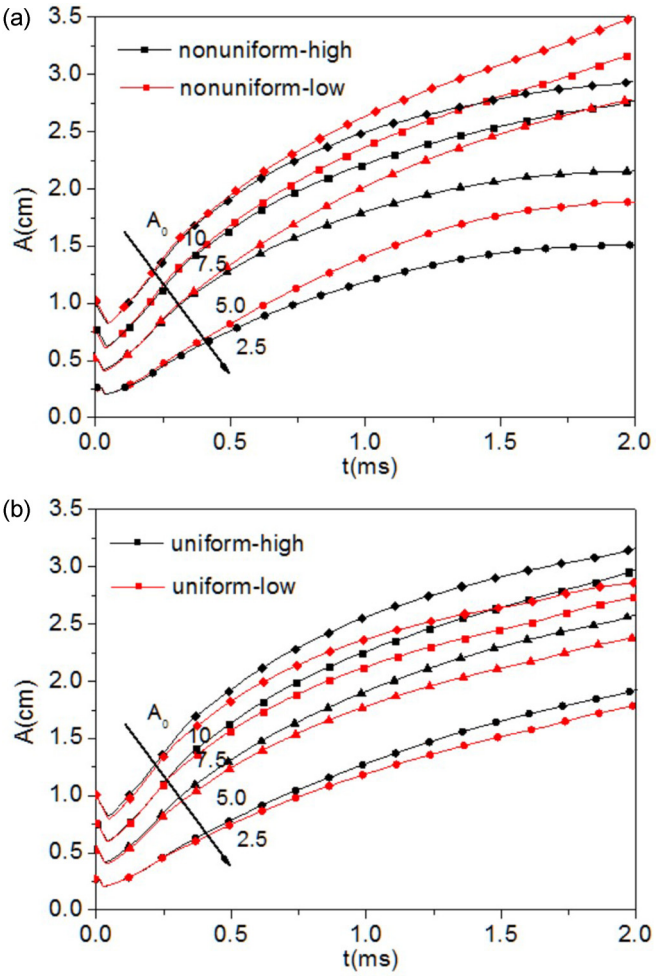

FIG. 7. Perturbation amplitudes of four different initial amplitudes: 2.5 (circles), 5 (triangles), 7.5 (squares), and 10 (diamonds) mm in (a) low- [red (light gray) lines] and high- (black lines) density zones of nonuniform flows and (b) low- [red (light gray) lines] and high- (black lines) density zones in uniform flows.

simulation results, high-density uniform flow simulation results, and nonuniform Gaussian function case. Each row corresponds to one group of initial amplitudes: (a) $A_{01} = 2.5$ mm-$A_{02} = 7.5$ mm, (b) $A_{01} = 5.0$ mm-$A_{02} = 7.5$ mm, (c) $A_{01} = 7.5$ mm-$A_{02} = 7.5$ mm, and (d) $A_{01} = 7.5$ mm-$A_{02} = 10.0$ mm.

The first observation is that the initial amplitude perturbation in both low-density and high-density uniform flows is significant, which means that the interface with larger initial amplitude develops faster than the smaller one. Additionally, there is subtle difference in the shape and structure of the bubble and spike between the low-density and high-density simulations with the same initial amplitude perturbation.

Nevertheless, the simulation results of nonuniform flow show a vital difference. The interface with the smaller initial amplitude in the low-density zone (upper channel) catches and even leaves behind the interface with the larger initial amplitude in the high-density zone (lower channel). Compared to Fig. 5 ($t = 1.8$ ms), this trend seems to be more distinctive over time.

Figure 4 and 5 demonstrate that the nonuniformity of the initial flow field has a vitally significant effect on Richtmyer-Meshkov instability. To figure out the mechanism of this interesting phenomenon, further discussion and analysis are needed in the following sections.

2. Amplitude

To further study the influence of nonuniformity, initial amplitude, and density on the evolution of interface instability, we analyzed the perturbation amplitude under different initial conditions. The interaction effect between two initial amplitudes should be taken into consideration first.

The definition of amplitude is given by $A(t) = [x_b(t) - x_s(t)]/2$, where x_b is the bubble position and x_s the corresponding spike position. Figure 6 depicts how the perturbation amplitude with the same initial amplitude ($A_0 = 7.5$ mm) varies when changing another initial amplitude under four different

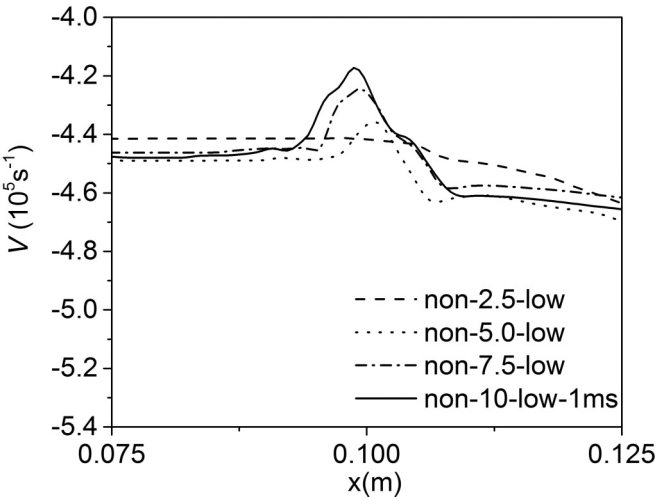

FIG. 8. Average vorticity of S3 (spike trough) in the low-density zone of nonuniform flows with four different initial amplitudes: 2.5 (dashed line), 5 (dotted line), 7.5 (dash-dotted line), and 10 (solid line) mm at $t = 1$ ms.

flow fields (low- and high-density zones in nonuniform flows and low- and high-density uniform flows). As can be seen, though with a slight difference at the late stage, the perturbation amplitudes of the same initial amplitude are almost the same in four flow fields, which indicates that the interaction between two different initial amplitudes is extremely weak.

Given the previous finding, we elected one-set data for an initial amplitude in the specific flow field to analyze the change of perturbation amplitude under the effect of nonuniformity and initial perturbation amplitude. Figure 7 demonstrates the perturbation amplitude under two initial conditions: (a) nonuniform flow and (b) uniform flow. First, we conducted the single-variable analysis. It can be seen that in the whole flow field with the identical density, an increase of initial perturbation amplitude A_0 results in greater amplitudes.

As for the condition of the same initial perturbation amplitude A_0 in different flow fields, it is evident that the evolution of the interface instability is closely linked to the flow nonuniformity. In Fig. 7(a), the result shows that the interface instability in a low-density area evolves faster than that in a high-density area, which is in striking contrast with

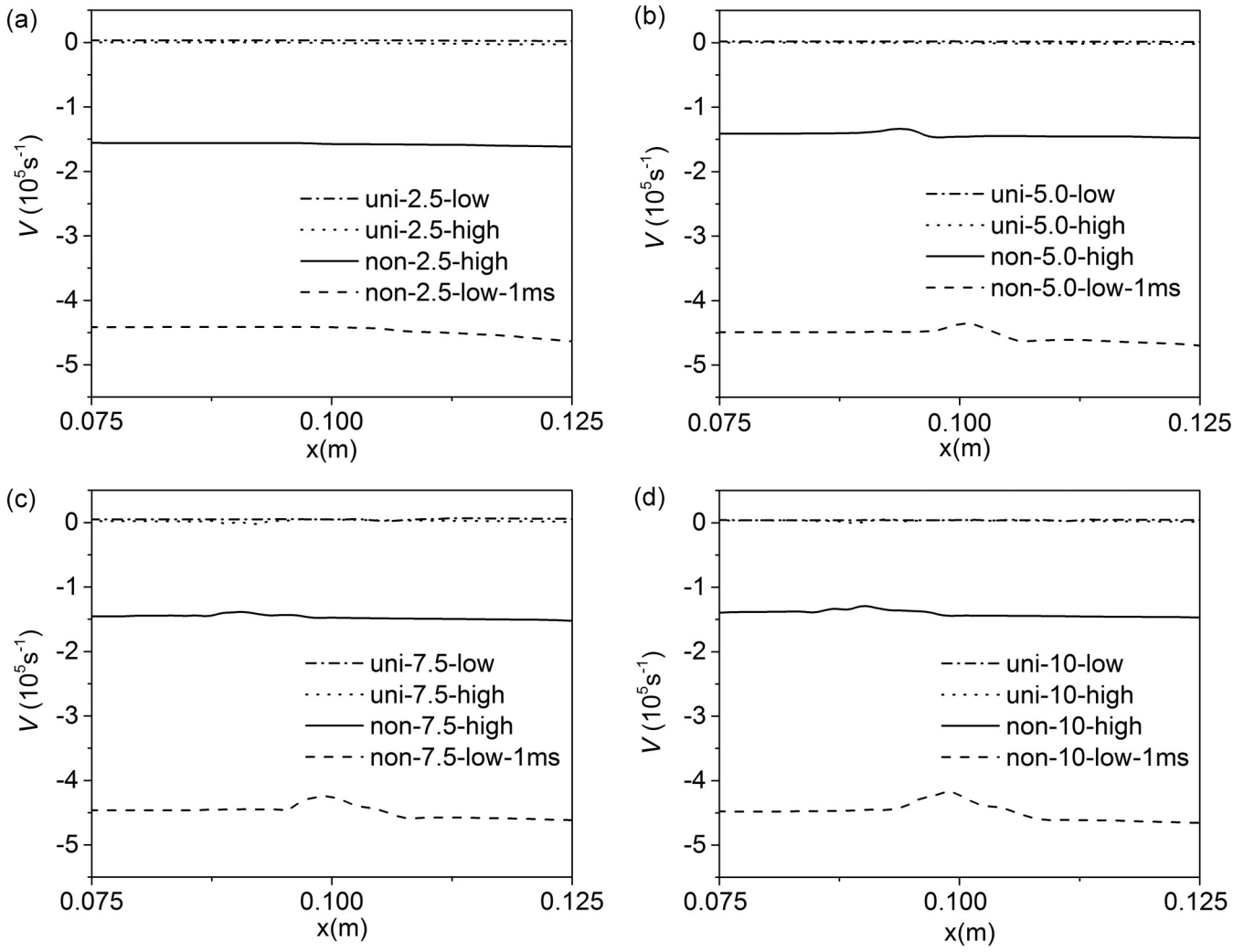

FIG. 9. Average vorticity of four conditions: the spike trough in low-density zone of nonuniform flows S3 (dash line), the spike trough in high-density zone of nonuniform flows S1 (solid line), and the spike trough in low-density uniform flows (dash-dotted line) and high-density uniform flows (dotted line) with four initial amplitudes (a) 2.5, (b) 5, (c) 7.5, and (d) 10 mm at $t = 1$ ms.

the evolution mechanism in the uniform flows, which can be concluded in Fig. 7(b). In addition, an interesting phenomenon can be observed in Fig. 7(a). In nonuniform flows, the amplitude growth of a smaller initial amplitude $A_0 = 5\,\text{mm}$ in a low-density zone catches the amplitude growth with an initial amplitude $A_0 = 7.5\,\text{mm}$ in a high-density zone at the late time of a nonlinear regime.

3. Vorticity

The growth of the Richtmyer-Meshkov instability evolution is caused by the decomposition vorticity that represents the curl of the velocity. The vorticity in the two-dimensional flow field is defined by the following equation:

$$\omega(x,y,t) = (\vec{\nabla} \times \vec{V}) \cdot \vec{n} = \partial v/\partial x - \partial u/\partial y, \qquad (4)$$

where $\vec{V}$ is the two-dimensional velocity vector and u and v are the velocity of the x and y components, respectively. We compared the vorticities of the trough of S1 and S3 and found that, when $t = 1\,\text{ms}$, the average position of the spike trough is about $x = 0.1\,\text{m}$. To find the accurate trough vorticity, we calculated the average vorticity of 50 grid cells above and below the trough plotted in Figs. 8 and 9. Specifically, the average vorticity is calculated in the domains $y \in [0.025, 0.075]$ and $y \in [0.125, 0.175]$.

Figure 8 reveals that the vorticity takes different values when the initial amplitudes are 2.5, 5, 7.5, and 10 mm. At the position of $x = 0.1\,\text{m}$, the vorticities reach -4.42×10^5, -4.35×10^5, -4.24×10^5, and $-4.17 \times 10^5\,\text{s}^{-1}$, respectively. In line with the trend of the amplitude, the increase of the initial amplitude leads to the rise of the vorticity.

Figure 9 exhibits the vorticity with the same initial amplitude in three distinctive density zones including low- and high-density uniform flows and low- and high-density zones in the nonuniform flow field. The absolute value of the average vorticity under four initial amplitudes in the low- and high-density uniform flows is about zero, yet the vorticity in the high-density zone of nonuniform flows rises to $1.5 \times 10^5\,\text{s}^{-1}$ and the low-density one even climbs to $4.5 \times 10^5\,\text{s}^{-1}$. It is apparent that the nonuniformity of the flows boosts the vorticity. Moreover, comparing Figs. 2 and 9, the density gradient of the low-density zone in the nonuniform flows is $-0.112\,\text{g/cm}^4$, much higher than the $-0.031\,\text{g/cm}^4$ in the high-density zone, which is a highly likely reason for the increase of the vorticity that promotes the evolution of the interface instability.

4. Circulation

Avoiding the contingency of the spike troughs' vorticity, the deposition of circulation is also available to quantify the mechanism of the interface instability. Circulation is the integral of the velocity vector along a closed curve. After Stokes's theorem is applied, circulation can be transformed to the vorticity integral in an area A, which is defined as

$$\Gamma(t) = \oint \vec{V} d\vec{l} = \int_A \omega(x,y,t) dA. \qquad (5)$$

The circulation of high and low zones in nonuniform flows is calculated in the same area: in the lower channel $[-0.02\,\text{m}, 0.25\,\text{m}] \times [0.0\,\text{m}, 0.0875\,\text{m}]$ and upper channel

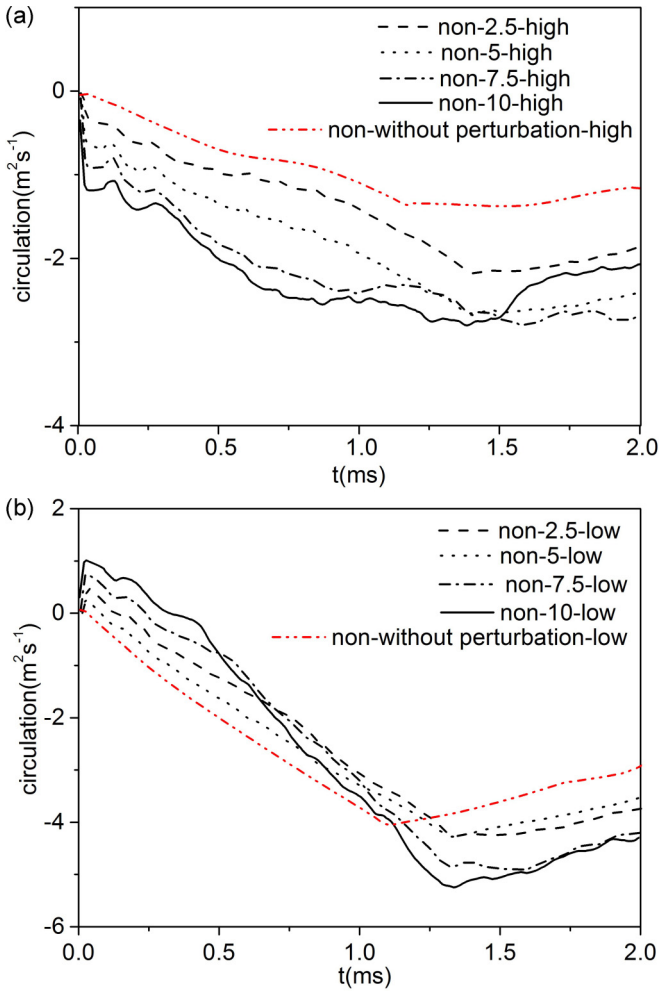

FIG. 10. Total circulation over time with four different initial amplitudes: 0.0 [red (light gray) dash–double-dotted line], 2.5 (dashed line), 5 (dotted line), 7.5 (dash-dotted line), and 10 (solid line) mm in (a) the low-density zone and (b) the high-density zone of nonuniform flows.

$[-0.02\,\text{m}, 0.25\,\text{m}] \times [0.1125\,\text{m}, 0.20\,\text{m}]$). Figure 10 shows the total circulation evolution over time. Data can be drawn from Fig. 6(a), that at the time $t = 1\,\text{ms}$, when the initial amplitudes are 0.0, 2.5, 5, 7.5, and 10 mm, the total circulations are -3.75, -3.12, -3.20, -3.34, and $-3.61\,\text{m}^2\,\text{s}^{-1}$, respectively, in the low-density zone of the nonuniform flow field. As for the high-density zone, the total circulations of different initial amplitudes are -1.13, -1.45, -1.95, -2.41, and $-2.52\,\text{m}^2\,\text{s}^{-1}$, respectively.

It can be summarized that the total circulation rises as the initial amplitude increases in the same density flow field, which is in concordance with the tendency of the vorticity. In particular, as for the case of a nonperturbation interface ($A_0 = 0.0\,\text{mm}$), the transverse gradient of nonuniform flows leads to a deposition of circulation that is smaller than the case of an interface with initial perturbation. This result underlines the effect of initial perturbation on the Richtmyer-Meshkov instability.

Figure 11(a) consists of positive circulation Γ^+, negative circulation Γ^-, and total circulation $\Gamma = \Gamma^+ + \Gamma^-$. It is

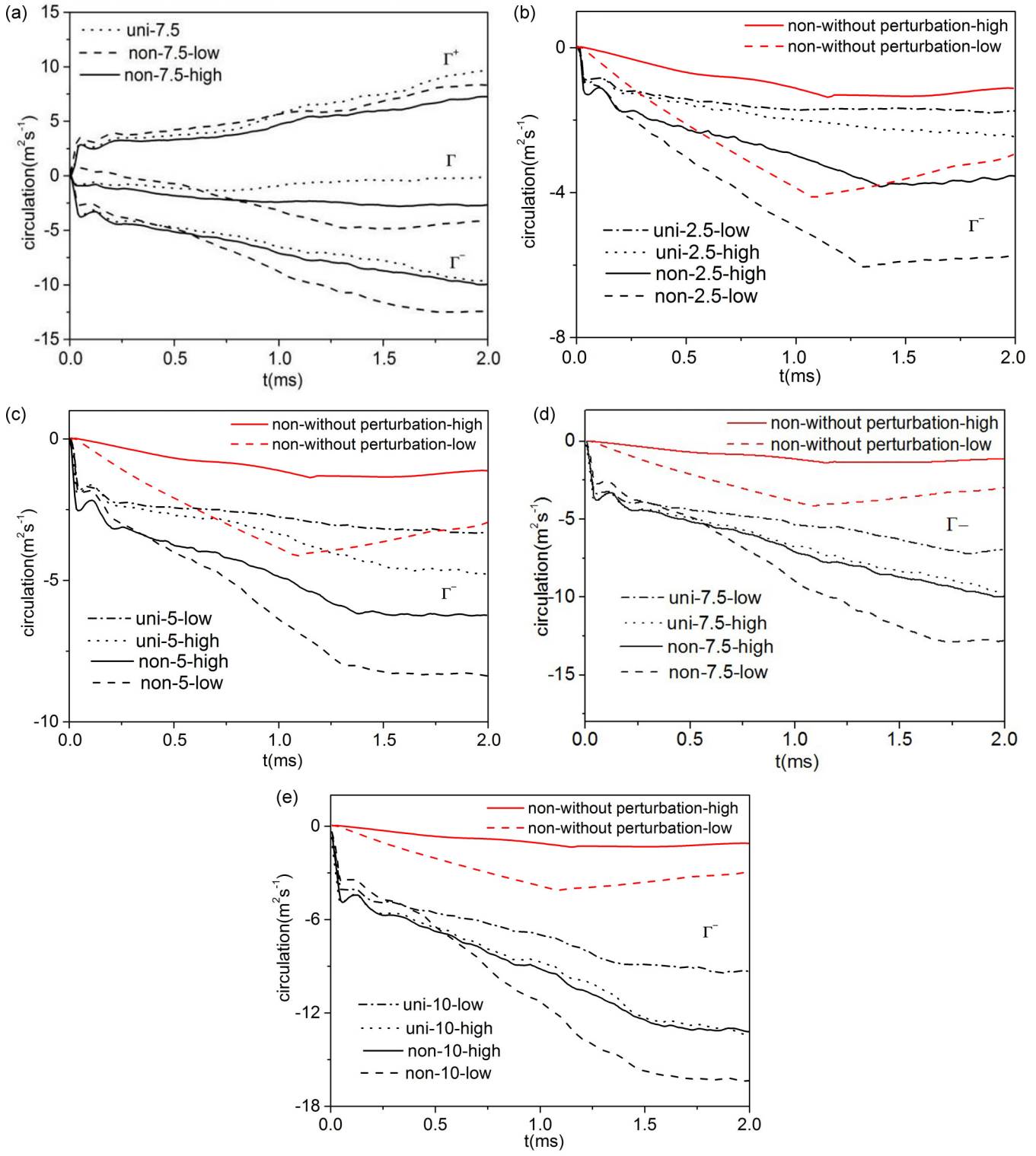

FIG. 11. Circulation over time in four conditions: the low-density zone of nonuniform flows (dashed line), the high-density zone of nonuniform flows (solid line), low-density uniform flows (dash-dotted line), and high-density uniform flows (dotted line) under four initial amplitudes: (a) 7.5 mm, (b) 2.5 mm (black lines) and 0.0 mm [red (light gray) lines], (c) 5 mm (black lines) and 0.0 mm [red (light gray) lines], (d) 7.5 mm (black lines) and 0.0 mm [red (light gray) lines], and (e) 10 mm (black lines) and 0.0 mm [red (light gray) lines].

clear that in Fig. 11(a), Γ in the uniform flows is about zero. Additionally, Γ^- dominates the total circulation in the nonuniform flows, thus analyzing Γ^- in the following section. More details about Γ^- in the low- and high-density uniform flows and the low- and high-density zones in the nonuniform flows are summarized in Table III.

At the moment $t = 1$ ms, $A_0 = 2.5$ mm, the negative circulations in the low- and high-density uniform flows, and

TABLE III. Negative circulations of five initial amplitudes in three flow fields at $t = 1$ ms.

A_0 (mm)	Negative circulation uniform low-density flow ($m^2\ s^{-1}$)	Negative circulation uniform high-density flow ($m^2\ s^{-1}$)	Negative circulation nonuniform high-density flow ($m^2\ s^{-1}$)	Negative circulation nonuniform low-density flow ($m^2\ s^{-1}$)
2.5	−1.02	−1.96	−2.94	−5.01
5	−2.72	−3.43	−4.93	−6.55
7.5	−5.37	−6.53	−7.07	−8.81
10	−6.91	−8.79	−9.23	−11.40
0.0	0.00	0.00	−0.35	−3.42

the high- and the low-density zone in the nonuniform flows are −1.02, −1.96, −2.94, and −5.01 $m^2\ s^{-1}$, which is consistent with the vorticity change. Given four other cases $A_0 = 0.0$, 5, 7.5, and 10 mm in Table III and Figs. 7(b)–7(e), it can be concluded that both nonuniformity and initial perturbation on the interface boost the circulation and the interface in the low-density zone with a higher-density gradient has a larger circulation than the one in a high-density area.

According to the quantitative analysis of amplitude, vorticity, and circulation, the following three major conclusions are obtained. First, in both the uniform and the nonuniform flow fields, the increase of initial amplitudes leads to the increase of amplitude, vorticity, and circulation. Next, the difference between the uniform and the nonuniform flow fields indicates that nonuniformity brings about a larger density gradient, which results in more deposition of vorticity and circulation. Finally, on the condition of the same initial amplitude, due to the higher-density gradient of the low-density zone in the nonuniform flow field, the amplitude, vorticity, and circulation are even higher than those in the high-density zone.

We believe that the above findings can illustrate the phenomena studied herein and will be useful for numerical and theoretical modeling for such complex flows.

IV. CONCLUSION

To sum up, through detailed simulations of the Richtmyer-Meshkov instability on the air-SF_6 interface under Ma = 1.27 shock and the uniform and nonuniform Gaussian function flows, initial perturbation effects on Richtmyer-Meshkov instability were quantitatively analyzed, which extends our prior work and explains the mechanism of the Richtmyer-Meshkov instability in the nonuniform flows. The distinctions between the uniform and nonuniform flow fields were clarified and an understanding of the nonuniformity effect was achieved. Moreover, our results demonstrated that the initial amplitudes have the same influence on the evolution of the interface disturbance in both the uniform and the nonuniform flows. As for various density conditions in the nonuniform flows, with the same initial amplitude, the interface evolution grows faster in the low-density zone than that in the high-density zone, which can be ascribed to a larger density gradient in its low-density area and which may have also resulted from the transmitted intensity of the incident shock at the interface. All in all, based on the conjunction of the initial amplitude and the nonuniformity, the evolution of the interface with a large initial amplitude in a low-density nonuniform zone appears to grow fastest and, on the other hand, the evolution with a small initial amplitude in a high-density nonuniform zone changes inversely.

On the strength of the present work, future work should be directed towards further study of the multimode coupled effects on interface instability in nonuniform flows. In addition, findings from this paper can serve as inspiring guidance for experimental studies such as forming the multimode interface with parallel growth rates in a nonuniform flow field.

ACKNOWLEDGMENTS

This research was supported by the National Natural Science Foundation of China under Grants No. 11372294 and No. 11532012 and the Foundation of National Key Laboratory of Shock Wave and Detonation Physics of China under Grant No. 9140C670301150C67290.

[1] J. Yang, T. Kubota, and E. E. Zukoski, AIAA J. **31**, 5 (1993).
[2] D. Arnett, Astrophys. J. Suppl. Ser. **127**, 213 (2000).
[3] P. Amendt, J. D. Colvin, R. E. Tipton, D. E. Hinkel, M. J. Edwards, O. L. Landen, J. D. Ramshaw, L. J. Suter, W. S. Varnum, and R. G. Watt, Phys. Plasmas **9**, 2221 (2002).
[4] S. Kumar, P. Vorobieff, G. Orlicz, A. Palekar, C. Tomkins, C. Goodenough, M. Marr-Lyon, K. P. Prestridge, and R. F. Benjamin, Physica D **235**, 21 (2007).
[5] G. C. Orlicz, B. J. Balakumar, C. D. Tomkins, and K. P. Prestridge, Phys. Fluids **21**, 064102 (2009).
[6] A. Malcolm, Los Alamos Laboratory Report No. LA-UR 11-02565, 2011 (unpublished).
[7] J. H. Liu, D. W. Tan, J. S. Bai, W. B. Wang, L.Y. Zou, and X. Zhang, J. Exp. Mech. **27**, 160 (2012).
[8] J. S. Bai, J. H. Liu, T. Wang, L.Y. Zou, P. Li, and D. W. Tan, Phys. Rev. E **81**, 056302 (2010).
[9] J. S. Bai, B. Wang, T. Wang, and K. Liu, Phys. Rev. E **86**, 066319 (2012).
[10] A. W. Vreman, Phys. Fluids **16**, 3670 (2004).
[11] T. Wang, J. S. Bai, P. Li, and M. Zhong, Chinese Phys. B **18**, 1127 (2009).